ACS APPLIED MATERIALS & INTERFACES

Research Article

Cite This: ACS Appl. Mater. Interfaces 2019, 11, 14191−14199

www.acsami.org

# $CsPbBr_3$ Quantum Dot Films with High Luminescence Efficiency and Irradiation Stability for Radioluminescent Nuclear Battery Application

Zhiheng Xu, Xiaobin Tang,* Yunpeng Liu, Zhengrong Zhang, Wang Chen, Kai Liu, and Zicheng Yuan

Department of Nuclear Science and Engineering, Nanjing University of Aeronautics and Astronautics, Nanjing 211106, China

Supporting Information

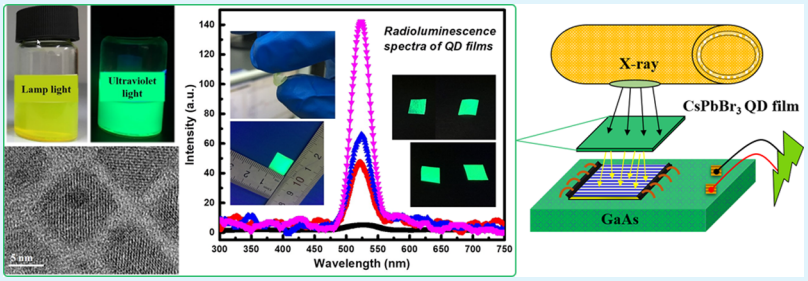


**ABSTRACT:** Highly luminescent $CsPbBr_3$ perovskite quantum dots (QDs) are very attractive for applications in power-generating devices. The $CsPbBr_3$ QD solution and its corresponding solid films were satisfactorily prepared. The obtained QDs were characterized by various techniques such as transmission electron microscopy, X-ray diffraction, ultraviolet−visible spectrophotometry, and photoluminescence and radioluminescence spectroscopy. The performance of the $CsPbBr_3$ QD films as an energy conversion material in radioluminescent nuclear batteries was analyzed and discussed. The output performance of different nuclear batteries based on $CsPbBr_3$ QD films was compared and the feasibility and advantages of using them as radioluminescent layers were investigated. On this basis, a long-term equivalent service behavior study was conducted to evaluate the irradiation stability of the $CsPbBr_3$ radioluminescent layer and predict the service life of this type of nuclear battery. The distribution state and penetration depth of hydrogen ions in the films were analyzed and evaluated using physics simulation software. Optical and electrical characteristics confirmed that this perovskite material could offer an efficient, stable, and scalable solution for energy conversion and photoelectric detection in the future.

**KEYWORDS:** *$CsPbBr_3$, perovskite quantum dots, energy conversion, X-ray, luminescence, nuclear battery, irradiation stability*

## 1. INTRODUCTION

Nuclear batteries, which convert particle radiation energy to electricity, have played an important role in many fields for power generation, such as pacemakers, underwater low-power systems, and equipment for exploring the outer planets.[1−3] Due to their high-energy density, extremely long life, and strong endurance under harsh conditions, nuclear batteries are a new type of energy with great potential for application. A radioluminescent nuclear battery, which is an extensively researched important branch of batteries nowadays, consists of three main components, namely, radiation sources, radioluminescent materials, and photovoltaic devices.[3−5] The usual conversion approach converts the radioisotope energy into photons via a phosphor and then converts these photons to electricity via a semiconductor junction device. Although the additional radioluminescence (RL) step may lead to a decrease in energy conversion efficiency, this approach can also protect the irradiation-sensitive semiconductors from lattice damage.[6−9] In order to improve the electrical properties of the radioluminescent nuclear batteries, the specification parameters and structural optimization of these three components have been extensively explored and summarized.[10−13] Numerous corresponding studies have also been carried out, such as using diverse energy conversion materials, optimizing the structure design, adopting a mixture of radioactive sources and phosphor layers, and adjusting the physical parameters.[14−16]

Previous studies have shown that it is a very effective measure to adopt a high-energy, high-activity excitation source, and superior energy conversion materials with high radioluminescence and photoelectric efficiency in improving the output power of the nuclear battery. Moreover, if there is a good coupling between the components, the performance output of the battery will be improved significantly.[17−19] These matches include the incident particle range approximating the thickness of the radioluminescent materials, the RL spectra consistent with the photovoltaic response interval of the photovoltaic devices. The radioactive source itself can continuously release energy. However, during the actual

Received: February 7, 2019
Accepted: March 28, 2019
Published: March 28, 2019






DOI: 10.1021/acsami.9b02425
ACS Appl. Mater. Interfaces 2019, 11, 14191−14199

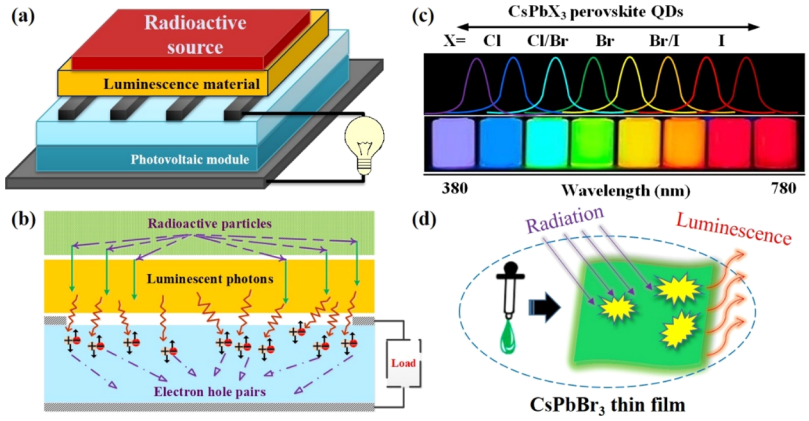


**Figure 1.** (a) 3D schematic structure and (b) working principle of the fabricated radioluminescent nuclear battery. (c) A series of typical luminescence spectra and photographs of $CsPbX_3$ (X = Cl, Br, and I) perovskite QDs. (d) Preparation of $CsPbBr_3$ QDs into a thin film and its RL.

application, the service life of the transducing material is an important factor that categorically determines the effective working time of the battery, especially for the radioluminescent material directly irradiated by the radioactive particles.

After decades of development, conventional phosphors, such as metal-doped zinc sulfide matrices and rare-earth-doped metal oxides, used for nuclear batteries have reached a certain bottleneck. In recent years, artificial semiconductor quantum dots (QDs) have attracted attention and presented many technological applications for new types of light-emitting displays, optoelectronic devices, and radiation detectors. QDs are characterized using a wide absorbance spectrum, large absorption cross-section, high quantum yield, and excellent photostability, which can control and manipulate the luminescence behavior.[20−23] Different emission peak wavelengths can also be obtained by altering the particle size or material composition of the QDs.[24−27] This feature breaks the limitations of traditional radioluminescent materials and increases the feasibility of matching. Based on their unique physical and chemical properties, QDs have significant application values in the field of radiation energy conversion. Considering the luminescence characteristics induced by radioactive particles (such as beta-particles and X-ray) and the excellent radiation stopping power of the all-inorganic halide perovskite $CsPbBr_3$ QDs, this type of nanomaterials may be very good candidates for radioluminescent nuclear batteries.[28−30]

In this study, the feasibility of using $CsPbBr_3$ as a radioluminescent nanostructured film under beta-particle or X-ray excitation was examined (Figure 1). The choice of nanomaterials has the hidden advantage of being able to convert radiation into precisely tuned luminous wavelengths that match the optimal wavelength for photovoltaic devices to be best converted into electricity, which will render the new system considerably more efficiency than previous traditional models. Specifically, $CsPbBr_3$ QDs were synthesized using the hot-injection technique and characterized under radiation particle excitation. The irradiation stability of the material was also presented.

## 2. RESULTS AND DISCUSSION

**2.1. Morphology and Optical Characterization.** Figure 2 illustrates the transmission electron micrographs of the $CsPbBr_3$ perovskite QDs. The morphologies of the $CsPbBr_3$ QDs were clearly observed. The QDs had a uniform size with a

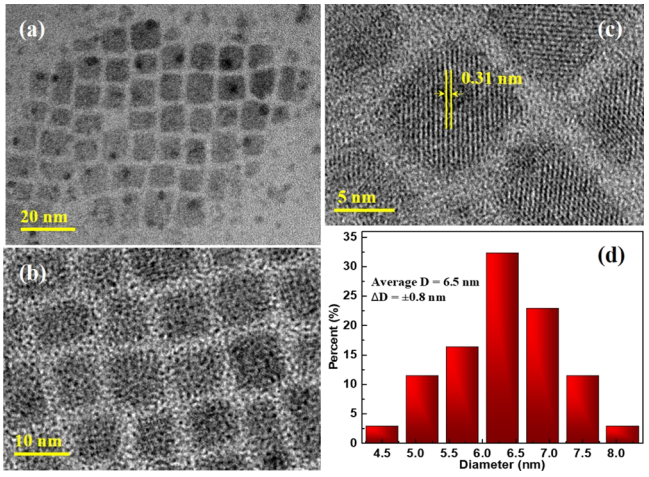


**Figure 2.** (a−c) Transmission electron micrographs and (d) particle size histogram of CsPbBr3 QDs. The scale bars are 20, 10, and 5 nm for (a−c).

regular square structure. The as-obtained cubic QDs had high crystalline quality and favorable monodispersity in solution, which is in well-accordance with published results.[31−35] The detailed size distribution of the QDs was calculated by transmission electron microscopy measurements, and the average diameter was estimated to be 6.5 nm with a size deviation of 0.8 nm. Figure 2d shows distinct lattice fringes of $CsPbBr_3$ QDs representing an interplanar distance of approximately 0.31 nm. In X-ray diffraction (XRD) spectra, significant diffraction peaks can be observed, and strong intensity diffraction peaks indicate the preferred orientation of nucleation formation and growth (Figure 3). The XRD patterns are in very good agreement with the XRD spectrum of a typical perovskite crystal structure. The peak positions of the two correspond to each other, indicating that the synthesized $CsPbBr_3$ QDs have a uniform composition and no other phases, which is suitable for crystal growth.[35−37] At the same time, the result further confirms the cubic structure and high crystallinity of the prepared $CsPbBr_3$ QDs.

The optical properties of $CsPbBr_3$ QDs were further investigated. The absorption and photoluminescence (PL) spectra in Figure 4 show the absorption edge at about 507 nm and a strong and symmetrical PL peak centered at 518 nm. The PL signal was quite narrow and with a full width at half-maximum of 18 nm. In addition, the band gap values $E_g$ (eV)


DOI: 10.1021/acsami.9b02425
ACS Appl. Mater. Interfaces 2019, 11, 14191−14199

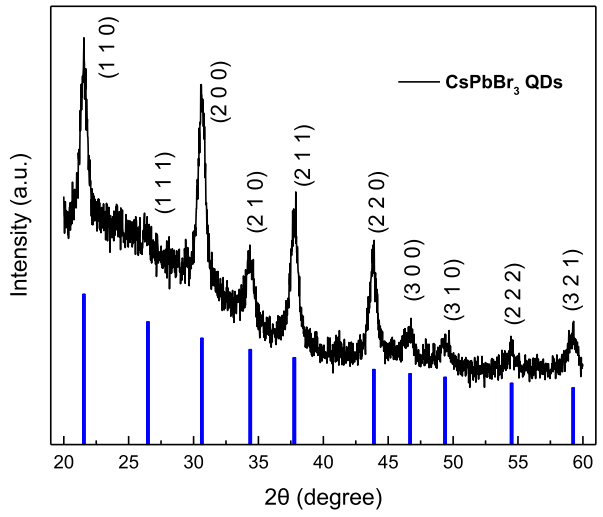


**Figure 3.** XRD patterns of $CsPbBr_3$ QDs compared with the theoretical diffraction pattern.

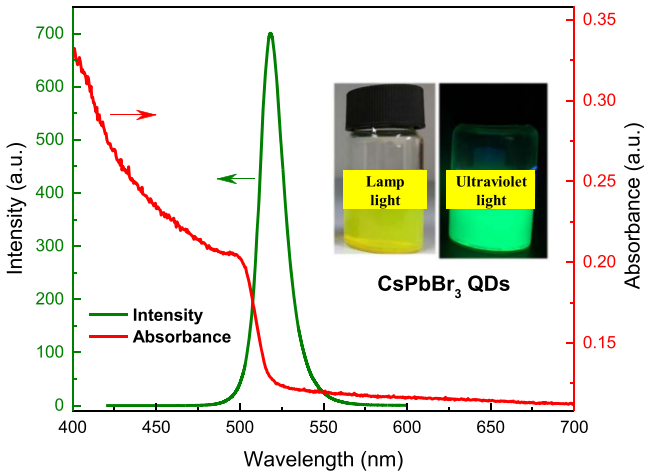


**Figure 4.** Optical absorption and steady-state PL emission spectra of $CsPbBr_3$ QDs dispersed in toluene. The inset shows the photographs of the QD sample under normal indoor light and UV light (365 nm) illumination, respectively.

of $CsPbBr_3$ QDs were calculated from the spectral curves and empirical formula as follows

$$E_g = hc/\lambda \quad (1)$$

where $h$ is Planck's constant ($4.1357 \times 10^{-15}$ eV·s); $c$ is the speed of light ($2.9979 \times 10^8$ m/s); and $\lambda$ is the wavelength (m) extracted from the absorption and PL spectra. A comparison of the wavelengths and the corresponding band gap values from Table 1 shows that the absorption edge position slightly deviated from the luminescence peak position, which is consistent with the Stokes shift effect in previous studies. The test results and bright purple PL emission

**Table 1. Band Gap Values for $CsPbBr_3$ QDs Calculated from Absorption and PL Emission Spectra**

| compound | absorption edge (nm) | $E_g$ calculated from absorption spectra (eV) | PL peak position (nm) | $E_g$ calculated from PL spectra (eV) |
|---|---|---|---|---|
| $CsPbBr_3$ | 507 | 2.446 | 518 | 2.394 |

indicated the high quality of $CsPbBr_3$ QDs synthesized by the hot-injection method.

**2.2. PL and RL Properties of $CsPbBr_3$ QD Films.** We fabricated and comprehensively investigated the $CsPbBr_3$ QD films with a tunable thickness. The polymerization and spinning method is a versatile technique to prepare QD films by mixing with polymethylmethacrylate (PMMA). The fluorescence spectra of $CsPbBr_3$ QD films were recorded in the visible light range at room temperature. The PL spectra of $CsPbBr_3$ QD films with different thicknesses and the effect of beta-irradiation on luminescence properties and X-ray-induced luminescence properties were studied, and the results are presented in Figure 5. Table 2 shows specific parameters of the $CsPbBr_3$ QD films and the corresponding experimental conditions. Further characteristic analysis such as absorption spectrum and transmission spectrum were performed, as shown in Figure S1.

Although varied luminescence intensities were exhibited by the QD films with different thicknesses, the same clear and strong emission wavelength at approximately 520 nm green light was observed under fluorescence and radiation excitation. The emission intensity increased with the thicknesses of the $CsPbBr_3$ QD films. Importantly, the maximum intensity at 520 nm was associated with a mean light photon energy of 2.38 eV. No noticeable changes were observed in the band centered position of QD solutions and QD films. However, the radioluminescence intensity of the $CsPbBr_3$ QD films under beta excitation was very weak. This phenomenon may be due to the lower activity of the beta source and the lower particle emission rate of the surface. Previous studies showed that the luminescence intensity can be significant with increased irradiation intensity.[9,17] Considering the available source conditions in the current laboratory, the X-ray emitting device exhibited good experimental results and could be used for subsequent effect testing and regular analysis. The prepared QD films showed a good flexible bending effect, which could greatly expand the application of these films. These results showed that the $CsPbBr_3$ perovskite QD films exhibited good RL and reproducibility. The steady RL properties of the $CsPbBr_3$ QD films substantiate the feasibility of the films as luminescence display and their promising potential for energy conversion.

**2.3. $CsPbBr_3$ QD Films Used in Radioluminescent Nuclear Batteries.** Based on the above optical experimental results, a new type of radioluminescent nuclear battery based on a $CsPbBr_3$ QD film was prepared. The $CsPbBr_3$ perovskite QD film acted as a transducer, converting the beta-particles or X-rays to visible light. Then, visible light was captured using a photovoltaic device, such as gallium arsenide (GaAs) or silicon (Si) solid-state semiconductors, and an electrical signal was generated and recorded. The films were added to elevate the energy conversion and transmission behavior between the excitation source and the photovoltaic device. Figure S2 displays the experimental equipment and test control interfaces. The beta sources used were consistent with the sources used for the RL test in Section 2.2. X-rays were radiated free-in-air using 25 and 50 kV tube voltages and 0.5 and 1.0 mA tube currents, respectively. High-conversion efficiency GaAs with 1 $cm^2$ effective area was selected as the photovoltaic device for this study. The external quantum efficiency curve of the GaAs photovoltaic device is compared with the RL spectrum of the $CsPbBr_3$ QD film, as detailed in the Supporting Information (Figure S3).



DOI: 10.1021/acsami.9b02425
ACS Appl. Mater. Interfaces 2019, 11, 14191−14199

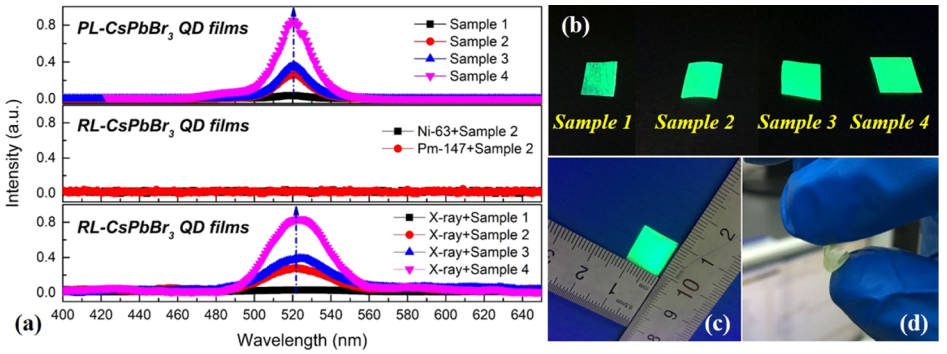


**Figure 5.** (a) PL and RL emission spectra of $CsPbBr_3$ QD films. (b) Photographs, (c) dimension, and (d) excellent bending demonstration of QD film samples. Sample 1, 2, 3, and 4 represent different samples, and the specific parameters are shown in Table 2.

**Table 2. Properties of $CsPbBr_3$ QD Films and Excitation Conditions of PL and RL**

| $CsPbBr_3$ QD films | film thickness ($\mu$m) | excitation condition | detailed parameter |
|---|---|---|---|
| sample 1 | 24.88 | excitation wavelength | ~390 nm |
| sample 2 | 69.19 | $^{63}$Ni source | 4.75 mCi/cm$^2$ |
| sample 3 | 103.90 | $^{147}$Pm source | 0.78 mCi/cm$^2$ |
| sample 4 | 151.14 | X-ray tube | tube voltage: 50 kV, tube current: 1 mA |

Figure 6 illustrates the measurement of the corresponding current−voltage ($I$−$V$) characteristics of different combinatorial nuclear batteries. The electrical output performance of the batteries under excitation by the beta sources was relatively weak in this experimental test. We also compared the electrical properties of two different cases without QD films (direct conversion, i.e., from radiant energy to electrical energy) and with $CsPbBr_3$ QD films (indirect conversion, i.e., from radiant energy to light energy to electrical energy). The optimal output performance is achieved with tradeoffs between the blocking effect of radiating particles, absorption of fluorescence photons, and light emission intensity of the QD films. For beta sources shown in Figure 6a, the $I$−$V$ curves of the batteries with and without films, and films with different mass thicknesses differed. The same radioluminescent materials and photovoltaic devices had different electrical output parameters under distinct beta source irradiation. Overall, the films did not significantly enhance the performance but even reduced the battery output. This result is consistent with previous optical test results.

Figure 6b shows a comparison of the current produced by the direct conversion with the same GaAs photovoltaic device as that by indirect conversion using the $CsPbBr_3$ QD films for X-rays under different tube voltages and tube currents. The maximum output power ($P_{max}$) of nuclear batteries can be extracted using eq 2 as follows

$$P_{max} = \mathrm{Max}(I \times V) = I_{mp}V_{mp} \quad (2)$$

where $P_{max}$ is the maximum value of the product of the current and voltage in the $I$−$V$ characteristic curves; and $I_{mp}$ and $V_{mp}$ are the current and voltage at the point of $P_{max}$, respectively. The short-circuit current ($I_{sc}$) corresponds to the short circuit condition when the impedance is weak, and this parameter is calculated when the voltage is zero. The variations in $I_{sc}$ and $P_{max}$ are demonstrated in Figure 7. The energy and amount of X-ray emitted and the electrical output of the battery increased with the tube voltage or current. The results of the experimental test showed that the $CsPbBr_3$ QD film increased the current output by 4.76% (from 4.11 to 4.31 $\mu$A) and the power output by 11.34% (from 1.19 to 1.34 $\mu$W) compared with the battery without films. For the determination of radiation excitation conditions and photovoltaic devices, the performance of QD films in the nuclear batteries was closely related to the corresponding RL conditions. The optimally chosen material parameters could evidently increase battery power (Figure S4). The results of radioluminescent nuclear batteries using the QD films as energy conversion materials were satisfactory, breaking the stereotype that direct conversion is necessarily superior to indirect conversion. This result also shows that $CsPbBr_3$ QD films have great

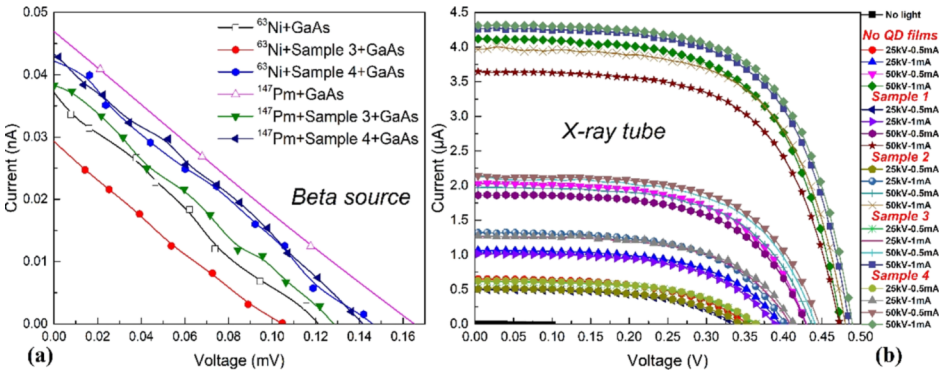


**Figure 6.** $I$−$V$ curves of several $CsPbBr_3$ QD film-based radioluminescent nuclear batteries. Excitation sources: (a) beta-source and (b) X-ray tube.



DOI: 10.1021/acsami.9b02425
ACS Appl. Mater. Interfaces 2019, 11, 14191−14199

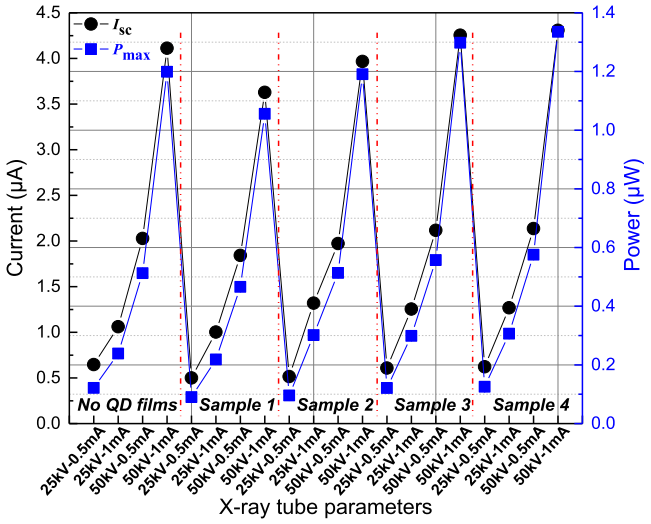


**Figure 7.** Short-circuit current $I_{sc}$ and maximum output power $P_{max}$ of radioluminescent nuclear batteries with different X-ray tube parameters.

application potential in the fields of radiation detection and photoelectric conversion.

**2.4. Irradiation Stability Tests of $CsPbBr_3$ QD Films.** Considering that $CsPbBr_3$ QD films were used in a radioactive environment, the RL behavior might cause a performance regression. The irradiation stability of $CsPbBr_3$ QD films during long-term energy conversion requires further clarification and investigation. To accelerate the irradiation experiment, we performed the proton irradiation in the QD films at the Institute of Modern Physics, Chinese Academy of Sciences. The films were irradiated by 150 and 200 keV hydrogen ions ($H^+$) with fluency ranging from $1.0 \times 10^{12}$ to $1.0 \times 10^{15}$ ions/cm$^2$ at room temperature, respectively. Figure 8 demonstrates that the $H^+$ ion with an energy of 150 and 200 keV will propagate at approximately 9.1 and 12.4 $\mu$m, respectively, in the $CsPbBr_3$ QD film and stop inside, as modeled and estimated using the Monte Carlo software SRIM. The $H^+$ concentration increased with the film depth, and the corresponding interstitial atoms and vacancies were gradually formed. Thus, numerous defects formed around the Bragg's peak. These defects produced abundant carrier traps and recombination centers, and further reduced the efficiency of energy conversion. Thus, the luminescence intensity was degraded.

Based on the simulation results and experimental processing conditions, four types of $CsPbBr_3$ QD films with different thicknesses were prepared and used to assess their stability under irradiation conditions. Table 3 provides the specific proton radiation parameters of the film samples. The optical properties of the film samples with varying thickness gradients were investigated before and after irradiation with different proton energy and fluence, respectively. Figure 9 illustrates the obtained optical transmission spectra. As the radiation parameters increased, the transmissivity of the films decreased. The higher the energy of irradiating particles, the more severe the effect on the films.

The RL spectra of the $CsPbBr_3$ QD films were treated under different conditions (Figure S5). The emission intensity increased for the films with an increase in X-ray irradiation parameters. The luminescence intensities of films with different thicknesses were inconsistent, but the regularities were consistent. The emission intensity decreased moderately after the $H^+$ ion irradiation. Figure 10 shows that the peaks of the luminescence intensity of the films treated with different techniques were compared under various X-ray tube parameters. The luminescence intensity has been enhanced by increasing the current or voltage of the X-ray tube. Based on certain two tube voltages, the enhancement degree of the luminescence intensity differed when the tube current was promoted from 0.5 to 1 mA. The higher the tube voltage was, the higher the promoted intensity. Similarly, for the two different tube currents, the larger the tube current, the greater the increase in the luminescence intensity as the tube voltage increased. A comparison of the optical output characteristics of films with different thicknesses showed the optimal thickness to achieve the best performance. For the same series of samples, the degradation of the optical performance increased as larger the energy or fluence parameter of proton irradiation. Hence, with the increase in X-ray tube parameters, the performance of the same series of film samples after the various irradiation conditions gradually increased. This result indicates that the stronger the radiative excitation conditions, the better the RL during energy conversion. These results are important to understand the radioluminescence properties of composites based on $CsPbBr_3$ QDs and to select the appropriate parameters of the excitation source and the composite QD films that would facilitate the attainment of high luminescence intensity.

The electrical performance of the irradiated $CsPbBr_3$ QD film samples for radioluminescent nuclear batteries was tested using various X-ray parameters at room temperature. After

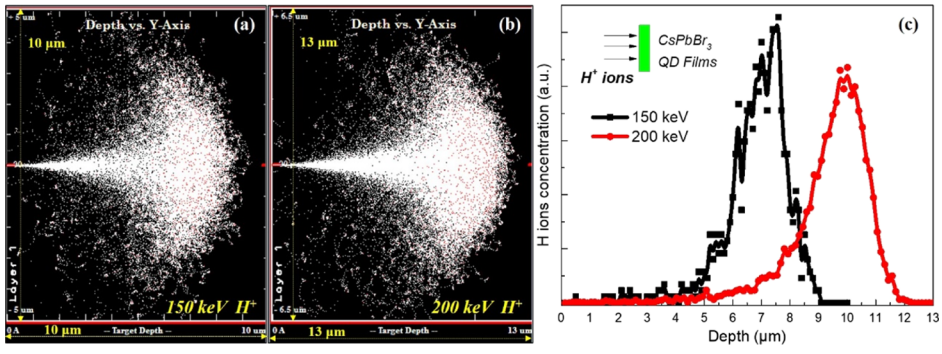


**Figure 8.** The distribution of (a) 150 keV and (b) 200 keV $H^+$ ions in the $CsPbBr_3$ QD films. (c) The penetration depth and $H^+$ concentration distribution in the film.



DOI: 10.1021/acsami.9b02425
ACS Appl. Mater. Interfaces 2019, 11, 14191−14199

**Table 3. Properties of $CsPbBr_3$ QD Films and Proton Radiation Parameters**

| sample thickness per type ($\mu$m) | sample number | radiation parameter | sample number | radiation parameter | sample number | radiation parameter |
|---|---|---|---|---|---|---|
| ~39 | 1 | stored at room temperature, without irradiation | 1# | $1.0 \times 10^{12}$ ions/cm$^2$, 150 keV | 1## | $1.0 \times 10^{12}$ ions/cm$^2$, 200 keV |
| ~115 | 2 | | 2# | $1.0 \times 10^{13}$ ions/cm$^2$, 150 keV | 2## | $1.0 \times 10^{13}$ ions/cm$^2$, 200 keV |
| ~166 | 3 | | 3# | $1.0 \times 10^{14}$ ions/cm$^2$, 150 keV | 3## | $1.0 \times 10^{14}$ ions/cm$^2$, 200 keV |
| ~215 | 4 | | 4# | $1.0 \times 10^{15}$ ions/cm$^2$, 150 keV | 4## | $1.0 \times 10^{15}$ ions/cm$^2$, 200 keV |

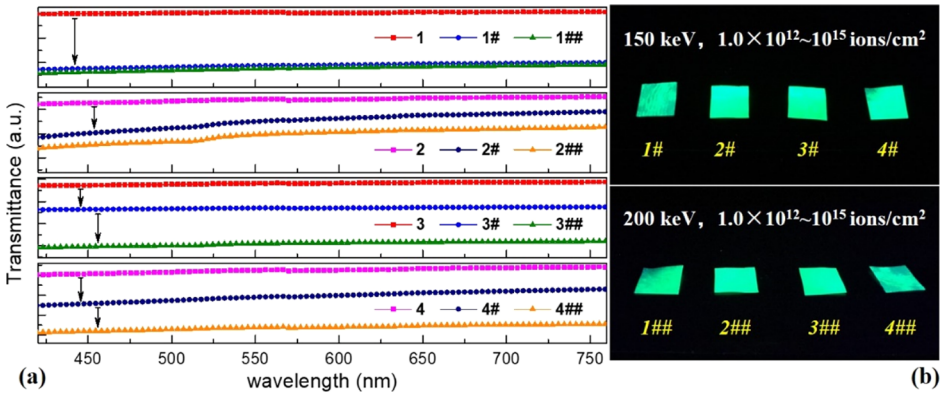


**Figure 9.** (a) Transmission spectra of the $CsPbBr_3$ QD films before and after irradiation, and (b) photographs of the irradiated QD films under UV light illumination. The numbers represent different samples and the specific parameters are shown in Table 3.

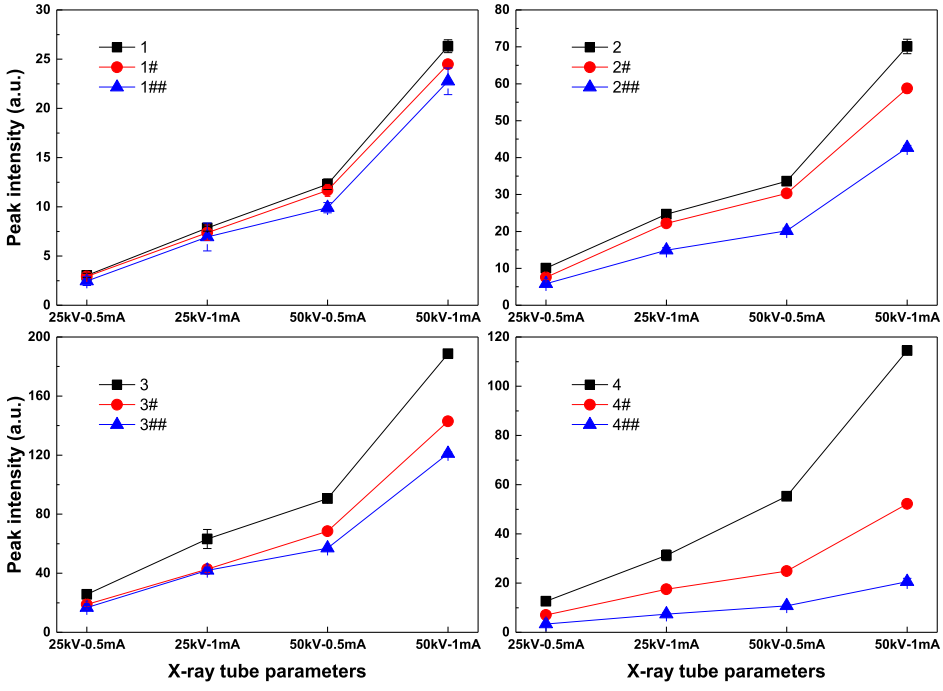


**Figure 10.** RL intensity contrast of several $CsPbBr_3$ QD films before and after irradiation.

processing the experimental data, a series of similar $I-V$ characteristic curves of the batteries are tested, and the current changed exponentially with the voltage (Figure S6). The open-circuit voltage ($V_{oc}$) was obtained when no current passed through the battery. The fill factor (FF) is essentially a measure of the quality of the nuclear battery. This parameter was calculated by comparing the maximum power to the theoretical power ($P_T$) that would be the output when $V_{oc}$ and $I_{sc}$ were considered together, as follows

$$\mathrm{FF} = \frac{P_{max}}{P_T} = \frac{I_{mp}V_{mp}}{I_{sc}V_{oc}} \quad (3)$$

Figure 11 shows the change in the corresponding electronic performance parameters for the battery with different $CsPbBr_3$ QD film samples. The degradation of the electrical performance was observed and evaluated after the proton irradiation with different energies and fluences. Overall, the $I_{sc}$ and $P_{max}$ fluctuated greatly within the range of 25−50 kV tube voltage



DOI: 10.1021/acsami.9b02425
ACS Appl. Mater. Interfaces 2019, 11, 14191−14199

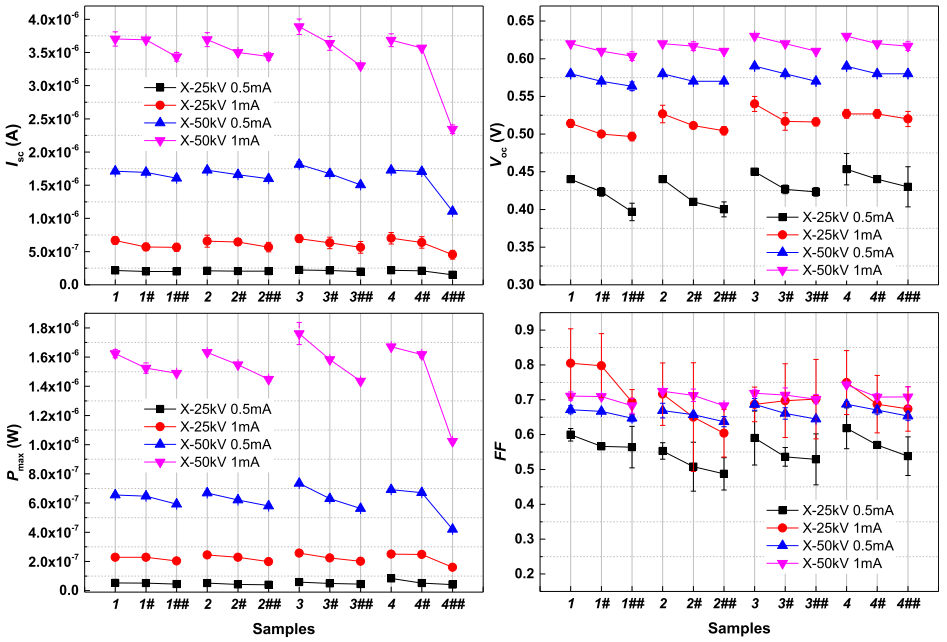


**Figure 11.** $I_{sc}$, $V_{oc}$, $P_{max}$, and FF of the radioluminescent nuclear batteries with different $CsPbBr_3$ QD film samples.

and 0.5−1 mA tube current. Moreover, in this range, the variations in the $V_{oc}$ and FF were relatively small and with similar trends. Analogous to previous radioluminescent test results, electrical performance was enhanced as the tube parameters were increased. The result of the present study was in agreement with that of a previous report.[9,17,30] In the same series of samples, more severe performance degradation was observed as the irradiation parameters were increased. $CsPbBr_3$ QD film-based radioluminescent nuclear batteries lost 8.29, 11.21, 18.52, and 38.75% (from 1, 2, 3, and 4 to 1##, 2##, 3##, and 4##) of the initial output power after irradiating with 200 keV protons with an integral fluence of $1.0 \times 10^{12}$ to $1.0 \times 10^{15}$ ions/cm$^2$, respectively. Thus, this type of nuclear battery will reduce the electrical performance output by 50% after approximately 755.87 days of continuous irradiation with conventional high energy and high activity beta sources for batteries. Moreover, if the energy or activity of the excitation source is higher, this life expectancy will be shortened accordingly. The minor variation in $V_{oc}$ and FF of $CsPbBr_3$ QD film-based radioluminescent nuclear batteries also indicates that the overall performance of the battery remained relatively stable and reliable after long-term irradiation. The results of the radiation stability tests reflect the degradation of the optical properties of the $CsPbBr_3$ QD films and the electrical properties in the nuclear battery. The results from the test data analysis show that the radiation resistance of the composite film samples was not poor. The results can also be utilized to evaluate film reliability and expected service life. The phenomena and mechanisms involved in the process have great potential in laser devices, luminescent displays, and portable power applications.

## 3. CONCLUSIONS

The excellent properties of $CsPbBr_3$ QDs prepared by the hot-injection method were verified by microscopic morphology characterization and optical test analysis. $CsPbBr_3$ QD films were obtained by uniformly mixing the QDs with PMMA solution, followed by spin coating and drying. In this work, the feasibility of using $CsPbBr_3$ QD films as a radioluminescent material in the nuclear battery was proved, and satisfactory results were obtained. Under suitable film parameters, the electrical output using the indirect energy conversion mode was higher than that using the direct energy conversion mode. Under the constant excitation source conditions, the output power of the battery with QD films could even be increased by 28.3%. The influence of proton irradiation resulted in the degradation in transmissivity, luminescence intensity, and electrical output. However, no significant changes in the peak position and emission spectrum pattern were observed, and the performance attenuation was not very remarkable. For a film of approximately 166 $\mu$m, exposure to 200 keV proton irradiation with a cumulative fluence of $1.0 \times 10^{15}$ ions/cm$^2$ reduced the RL intensity and the output power of the battery by approximately 35.86 and 18.52%, respectively, compared with those before irradiation. Moreover, the results from a series of comparative studies indicated that the degree of attenuation would be lower if the parameters of the excitation source and the film were properly selected. In future studies, different kinds and physical parameters of QDs may be explored to study the effect of wavelength regulation for the development of applications in optoelectronic devices and for radiation protection coating.

## 4. EXPERIMENTAL SECTION

**4.1. Preparation of $CsPbBr_3$ QD Films.** All-inorganic perovskite nanoparticles ($CsPbBr_3$) were synthesized by the traditional colloidal hot-injection method. $CsPbBr_3$ QDs were obtained by reacting CsBr with $PbBr_2$ in toluene solution. A long-term colloidal stable QD solution was obtained after low-temperature cooling nucleation, multiple centrifugation, and redissolution. $CsPbBr_3$ QDs and PMMA were dissolved in toluene solution and mixed by mechanical stirring. The mixed solution of QDs and PMMA with a volume ratio of 3:1 was formed as a solid transparent film with a spinner under vacuum conditions. The films were dried at 80 °C and subsequently cured to the desired size. The final QD film was mainly determined by slurry concentration, spin speed, and duration.

**4.2. Material Characterization and Property Measurements.** The crystal structure, morphology, and size distribution of $CsPbBr_3$



DOI: 10.1021/acsami.9b02425
ACS Appl. Mater. Interfaces 2019, 11, 14191−14199

QDs were characterized using a FEI Tecnai G2 transmission electron microscope operating at an acceleration voltage of 200 kV. The nanocrystals were deposited from the diluted solutions onto copper grids. The optical transmittance of the films in the visible-light region was measured with a Shimadzu 3600 UV−vis spectrophotometer. The steady and high-resolution PL spectra were recorded with a Cary Eclipse luminescence spectrophotometer (Agilent Technologies G9800a, Malaysia). The RL spectra from the beta or X-ray sources were recorded, and the luminescence spectrophotometer recorded the wavelength from 300 to 800 nm simultaneously at any given excitation energy. *I*−*V* curves were plotted using a semiconductor measuring instrument (Keithley 4200-SCS, USA), which provided valuable information on the electrical parameter characteristics of the nuclear batteries. The QD thin films were irradiated using 150 and 200 keV hydrogen ions with a fluence of $1.0 \times 10^{12}$ to $1.0 \times 10^{15}$ $cm^{-2}$, respectively. The cumulative dose effect changed the optical and electrical properties of the QD films. The optical luminescence tests, material irradiation experiments, and electrical output performance tests were conducted at room temperature around 298 K and one bar pressure.

## ■ ASSOCIATED CONTENT

### Supporting Information

The Supporting Information is available free of charge on the ACS Publications website at DOI: 10.1021/acsami.9b02425.

Absorption and transmission spectra of the $CsPbBr_3$ QD films, experimental instruments, and equipment; comparison of radioluminescence emission spectra and current−voltage curves before and after irradiation; comparison of specific electrical properties of nuclear batteries under different conditions; additional figure of spectral response; and results and discussion (PDF)

## ■ AUTHOR INFORMATION


### Corresponding Author

*E-mail: tangxiaobin@nuaa.edu.cn. Phone: +86 13601582233. Fax: (+86) 025-52112908-80407.

### ORCID

Xiaobin Tang: 0000-0003-3308-0468


### Notes

The authors declare no competing financial interest.

## ■ ACKNOWLEDGMENTS

This work was financially supported by the National Natural Science Foundation of China (grant no. 11675076). The authors thank Feng Tian and Pinyuan Xu for their technical help over the course of this study.

## ■ REFERENCES


(1) Bower, K.-E.; Barbanel, Y.-A.; Shreter, Y.-G.; Bohnert, G.-W. *Polymers, Phosphors, and Voltaics for Radioisotope Microbatteries*; CRC Press LLC: New York, 2002; pp 24−52.

(2) Liu, Y.; Tang, X.; Xu, Z.; Hong, L.; Wang, P.; Chen, D. Optimization and temperature effects on sandwich betavoltaic microbattery. *Sci. China: Technol. Sci.* **2014**, *57*, 14−18.

(3) Prelas, M. A.; Weaver, C. L.; Watermann, M. L.; Lukosi, E. D.; Schott, R. J.; Wisniewski, D. A. A Review of Nuclear Batteries. *Prog. Nucl. Energy* **2014**, *75*, 117−148.

(4) Sychov, M.; Kavetsky, A.; Yakubova, G.; Walter, G.; Yousaf, S.; Lin, Q.; Chan, D.; Socarras, H.; Bower, K. Alpha Indirect Conversion Radioisotope Power Source. *Appl. Radiat. Isot.* **2008**, *66*, 173−177.

(5) Kumar, S. Atomic Batteries: Energy from Radioactivity. arXiv preprint arXiv:1511.07427, **2015**; Vol. *1*−*8*.

(6) Cress, C. D.; Redino, C. S.; Landi, B. J.; Raffaelle, R. P. Alpha-Particle-Induced Luminescence of Rare-Earth-Doped $Y_2O_3$ Nanophosphors. *J. Solid State Chem.* **2008**, *181*, 2041−2045.

(7) Tang, X.-B.; Hong, L.; Xu, Z.-H.; Liu, Y.-P.; Chen, D. Temperature Effect of a Radioluminescent Nuclear Battery Based on $^{147}Pm$/ZnS: Cu/GaAs. *Appl. Radiat. Isot.* **2015**, *97*, 118−124.

(8) Russo, J.; Litz, M.; Ray, W.; Rosen, G. M.; Fazio, R. Radioluminescent Nuclear Battery Using Volumetric Configuration: $^{63}Ni$ solution/ZnS: Cu, Al/InGaP. *Appl. Radiat. Isot.* **2017**, *125*, 66−73.

(9) Zhang, Z.-R.; Liu, Y.-P.; Tang, X.-B.; Xu, Z.-H.; Yuan, Z.-C.; Liu, K.; Chen, W. GaAs Low-Energy X-Ray Radioluminescence Nuclear Battery. *Nucl. Instrum. Methods Phys. Res., Sect. B* **2018**, *415*, 9−16.

(10) Bailey, S.-G.; Wilt, D.-M.; Castro, S.-L.; Cress, C.-D.; Raffaelle, R.-P. Photovoltaic Development for Alpha Voltaic Batteries. *Conference Record of the Thirty-First IEEE Photovoltaic Specialists Conference*; IEEE: Lake Buena Vista, FL, Jan 3−7 2005; Vol. *106*−*109*.

(11) Raffaelle, R.-P.; Jenkins, P.; Wilt, D.; Scheiman, D.; Chubb, D.; Castro, S. Alpha Voltaic Batteries and Methods Thereof. U.S. Patent 7,718,283 B2, May 18, 2010.

(12) Guo, X.; Liu, Y.; Xu, Z.; Jin, Z.; Liu, K.; Yuan, Z.; Gong, P.; Tang, X. Multi-level Radioisotope Batteries Based on $^{60}Co$ $\gamma$ Source and Radio-Voltaic/Radio-Photovoltaic Dual Effects. *Sens. Actuators, A* **2018**, *275*, 119−128.

(13) Prelas, M. A.; Tchouaso, M. T. High efficiency Dual-Cycle Conversion System Using Kr-85. *Appl. Radiat. Isot.* **2018**, *139*, 70−80.

(14) Xu, Z.; Liu, Y.; Zhang, Z.; Chen, W.; Yuan, Z.; Liu, K.; Tang, X. Enhanced Radioluminescent Nuclear Battery by Optimizing Structural Design of the Phosphor Layer. *Int. J. Energy Res.* **2018**, *42*, 1729−1737.

(15) Hong, L.; Tang, X.-B.; Xu, Z.-H.; Liu, Y.-P.; Chen, D. Parameter Optimization and Experiment Verification for a Beta Radioluminescence Nuclear Battery. *J. Radioanal. Nucl. Chem.* **2014**, *302*, 701−707.

(16) Landis, G.-A.; Bailey, S.-G.; Clark, E.-B.; Myers, M.-G.; Piszczor, M.-F.; Murbach, M.-S. Non-solar Photovoltaics for Small Space Missions. *38th IEEE Photovoltaic Specialists Conference (PVSC)*; IEEE: New York, Austin, TX, June 3−8, 2012; pp 002819−002824.

(17) Hong, L.; Tang, X.-B.; Xu, Z.-H.; Liu, Y.-P.; Chen, D. Radioluminescent Nuclear Batteries with Different Phosphor Layers. *Nucl. Instrum. Methods Phys. Res., Sect. B* **2014**, *338*, 112−118.

(18) Tang, X.; Xu, Z.; Liu, Y.; Liu, M.; Wang, H.; Chen, D. Physical Parameters of Phosphor Layers and their Effects on the Device Properties of Beta-Radioluminescent Nuclear Batteries. *Energy Technol.* **2015**, *3*, 1121−1129.

(19) Jin, Z.; Tang, X.; Guo, X.; Liu, Y.; Xu, Z.; Chen, W.; Zhou, D. Design and Performance Study of Four-Layer Radio-Voltaic and Dual-Effect Nuclear Batteries Based on $\gamma$-ray. *Nucl. Instrum. Methods Phys. Res., Sect. B* **2018**, *428*, 47−55.

(20) Li, C.; Zang, Z.; Chen, W.; Hu, Z.; Tang, X.; Hu, W.; Sun, K.; Liu, X.; Chen, W. Highly Pure Green Light Emission of Perovskite $CsPbBr_3$ Quantum Dots and Their Application for Green Light-emitting Diodes. *Opt. Express* **2016**, *24*, 15071−15078.

(21) Li, C.; Zang, Z.; Han, C.; Hu, Z.; Tang, X.; Du, J.; Leng, Y.; Sun, K. Highly Compact $CsPbBr_3$ Perovskite Thin Films Decorated by ZnO Nanoparticles for Enhanced Random Lasing. *Nano Energy* **2017**, *40*, 195−202.

(22) Chen, W.; Tang, X.; Wangyang, P.; Yao, Z.; Zhou, D.; Chen, F.; Li, S.; Lin, H.; Zeng, F.; Wu, D.; Sun, K.; Li, M.; Huang, Y.; Hu, W.; Zang, Z.; Du, J. Surface-Passivated Cesium Lead Halide Perovskite Quantum Dots: Toward Efficient Light-Emitting Diodes with an Inverted Sandwich Structure. *Adv. Opt. Mater.* **2018**, *6*, 1800007.

(23) Chen, W.; Shi, T.; Du, J.; Zang, Z.; Yao, Z.; Li, M.; Sun, K.; Hu, W.; Leng, Y.; Tang, X. Highly Stable Silica-Wrapped Mn-Doped $CsPbCl_3$ Quantum Dots for Bright White Light-Emitting Devices. *ACS Appl. Mater. Interfaces* **2018**, *10*, 43978−43986.

(24) Medintz, I. L.; Uyeda, H. T.; Goldman, E. R.; Mattoussi, H. Quantum Dot Bioconjugates for Imaging, Labelling and Sensing. *Nat. Mater.* **2005**, *4*, 435−446.




DOI: 10.1021/acsami.9b02425
*ACS Appl. Mater. Interfaces* 2019, 11, 14191−14199

(25) Han, H.-V.; Lin, C.-C.; Tsai, Y.-L.; Chen, H.-C.; Chen, K.-J.; Yeh, Y.-L.; Lin, W.-Y.; Kuo, H.-C.; Yu, P. A Highly Efficient Hybrid GaAs Solar Cell Based on Colloidal-Quantum-Dot-Sensitization. *Sci. Rep.* **2015**, *4*, 5734.
(26) Yang, K.; Li, F.; Liu, Y.; Xu, Z.; Li, Q.; Sun, K.; Qiu, L.; Zeng, Q.; Chen, Z.; Chen, W.; Lin, W.; Hu, H.; Guo, T. All-Solution-Processed Perovskite Quantum Dots Light-Emitting Diodes Based on the Solvent Engineering Strategy. *ACS Appl. Mater. Interfaces* **2018**, *10*, 27374−27380.
(27) Mei, S.; Liu, X.; Zhang, W.; Liu, R.; Zheng, L.; Guo, R.; Tian, P. High-Bandwidth White-Light System Combining a Micro-LED with Perovskite Quantum Dots for Visible Light Communication. *ACS Appl. Mater. Interfaces* **2018**, *10*, 5641−5648.
(28) Chen, H.-C.; Lin, C.-C.; Han, H.-V.; Chen, K.-J.; Tsai, Y.-L.; Chang, Y.-A.; Shih, M.-H.; Kuo, H.-C.; Yu, P. Enhancement of Power Conversion Efficiency in GaAs Solar Cells with Dual-Layer Quantum Dots Using Flexible PDMS Film. *Sol. Energy Mater. Sol. Cells* **2012**, *104*, 92−96.
(29) Chen, W.; Liu, Y.; Yuan, Z.; Xu, Z.; Zhang, Z.; Liu, K.; Jin, Z.; Tang, X. X-ray Radioluminescence Effect of All-Inorganic Halide Perovskite $CsPbBr_3$ Quantum Dots. *J. Radioanal. Nucl. Chem.* **2017**, *314*, 2327−2337.
(30) Chen, W.; Tang, X.; Liu, Y.; Xu, Z.; Han, Z.; Zhang, Z.; Wang, H.; Peng, C. Novel Radioluminescent Nuclear Battery: Spectral Regulation of Perovskite Quantum Dots. *Int. J. Energy Res.* **2018**, *42*, 2507−2517.
(31) Swarnkar, A.; Chulliyil, R.; Ravi, V. K.; Irfanullah, M.; Chowdhury, A.; Nag, A. Colloidal $CsPbBr_3$ Perovskite Nanocrystals: Luminescence Beyond Traditional Quantum Dots. *Angew. Chem.* **2015**, *127*, 15644−15648.
(32) Wang, Y.; Li, X.; Song, J.; Xiao, L.; Zeng, H.; Sun, H. All-Inorganic Colloidal Perovskite Quantum Dots: a New Class of Lasing Materials with Favorable Characteristics. *Adv. Mater.* **2015**, *27*, 7101−7108.
(33) Castañeda, J. A.; Nagamine, G.; Yassitepe, E.; Bonato, L.-G.; Voznyy, O.; Hoogland, S.; Nogueira, A.-F.; Sargent, E.-H.; Brito Cruz, C.-H.; Pasilha, L.-A. Efficient Biexciton Interaction in Perovskite Quantum Dots Under Weak and Strong Confinement. *ACS Nano* **2016**, *10*, 8603−8609.
(34) Panigrahi, S.; Jana, S.; Calmeiro, T.; Nunes, D.; Martins, R.; Fortunato, E. Imaging the Anomalous Charge Distribution Inside $CsPbBr_3$ Perovskite Quantum Dots Sensitized Solar Cells. *ACS Nano* **2017**, *11*, 10214−10221.
(35) Shi, Z.; Li, S.; Li, Y.; Ji, H.; Li, X.; Wu, D.; Xu, T.; Chen, Y.; Tian, Y.; Zhang, Y.; Shan, C.; Du, G. Strategy of Solution-Processed All-Inorganic Heterostructure for Humidity/Temperature-Stable Perovskite Quantum Dot Light-Emitting Diodes. *ACS Nano* **2018**, *12*, 1462−1472.
(36) Tong, Y.; Fu, M.; Bladt, E.; Huang, H.; Richter, A. F.; Wang, K.; Müller-Buschbaum, P.; Bals, S.; Tamarat, P.; Lounis, B.; Feldmann, J.; Polavarapu, L. Chemical Cutting of Perovskite Nanowires into Single-Photon Emissive Low-Aspect-Ratio $CsPbX_3$ (X= Cl, Br, I) Nanorods. *Angew. Chem.* **2018**, *130*, 16326−16330.
(37) Tong, Y.; Yao, E.-P.; Manzi, A.; Bladt, E.; Wang, K.; Döblinger, M.; Bals, S.; Müller-Buschbaum, P.; Urban, A. S.; Polavarapu, L.; Feldmann, J. Spontaneous Self-Assembly of Perovskite Nanocrystals into Electronically Coupled Supercrystals: Toward Filling the Green Gap. *Adv. Mater.* **2018**, *30*, 1801117.


DOI: 10.1021/acsami.9b02425
*ACS Appl. Mater. Interfaces* 2019, 11, 14191−14199